Iron(III)-bipyridine incorporated metal-organic frameworks for photocatalytic reduction of CO2 with improved performance

Journal:	*Dalton Transactions*
Manuscript ID	DT-ART-10-2020-003500.R3
Article Type:	Paper
Date Submitted by the Author:	29-Nov-2020
Complete List of Authors:	Wei, Yuan-Ping; Nanjing University, Coordination Chemistry Institute Yang, Sizhuo; Marqutte University, Chemistry Wang, Peng; Nanjing University, Coordination Chemistry Institute Guo, Jin-Han; Nanjing University Huang, Jier; Marqutte University, Chemistry Sun, Wei-Yin; Nanjing University, Coordination Chemistry Institute

Journal Name

ARTICLE

Iron(III)-bipyridine incorporated metal-organic frameworks for photocatalytic reduction of CO_2 with improved performance†

Yuan-Ping Wei,[‡,a] Sizhuo Yang,[‡,b] Peng Wang,[a] Jin-Han Guo,[a] Jier Huang*[,b] and Wei-Yin Sun*[,a]

Metal-organic frameworks (MOFs) represent an emerging class of platforms to assemble single site photocatalyst for artificial photosynthesis. In this work, we report a new CO_2 reduction photocatalyst (UiO-68-Fe-bpy) based on a robust Zr(IV)-MOF platform with incorporated Fe(bpy)Cl₃ (bpy refers to 4′-methyl-[2,2′-bipyridine] moiety) *via* amine-aldehyde condensation. We show that this hybrid catalyst can reduce CO_2 to form CO under visible light illumination with excellent selectivity and enhanced activity with respect to its parent MOF and corresponding homogeneous counterpart. Using steady state and transient absorption (TA) spectroscopy, we show that the enhanced photocatalytic activity of UiO-68-Fe-bpy is attributed to the elongated excited state lifetime of Fe(bpy)Cl₃ after being incorporated to the UiO-68-NH₂ platform. This work demonstrates the great potential of MOFs as next generation platform for solar fuel conversion.

Introduction

With soared energy demand and intensified global warming, searching for effective conversion of CO_2 into valuable chemicals is an important but challenging task.[1-3] Inspired by nature, chemists express strong interest in the systems that can photocatalytically reduce CO_2 to the energy carrier products such as CH_4, CH_3OH, HCOOH and CO.[4] These systems include homogeneous transition-metal complexes,[5] heterogeneous metal-incorporated zeolites,[6] and inorganic semiconductors.[7-12] However, the homogeneous transition-metal complexes are often not recyclable although many of them show high efficiency in reducing CO_2 in the presence of photosensitizers.[13] On the other hand, the metal-incorporated zeolites and inorganic semiconductors are robust but often suffer from poor efficiency for photocatalytic reduction of CO_2.[14] Therefore, developing new photocatalysts with high efficiency and stability is necessary in order to convert CO_2 to useful chemical fuels.

Metal-organic frameworks (MOFs), constructed from metal ion or metal cluster nodes interconnected with organic ligands, are a class of crystalline micro-/meso-porous materials and have been explored for a variety of potential applications including drug delivery,[15,16] gas storage,[17-19] chemical separation and catalysis.[20-26] In particular, MOFs have shown great potential for photocatalytic CO_2 reduction via incorporating catalytic sites into porous and robust MOF matrix.[27-37] Among the systems reported, one valuable strategy is to incorporate organometallic species into MOFs through post synthetic modification (PSM), where the organometallic species serve as both photosensitizer and CO_2-reduction catalyst such that the photocatalytic system can take advantage of both homogenous and heterogeneous catalysts.[38-42] For example, molecular complexes based on noble metals such as platium, ruthenium and iridium have been incorporated to MOFs and demonstrate catalytic activity for photocatalytic CO_2 reduction.[43-45] Molecular complexes based on cost effective and earth abundant transition metals including iron, cobalt, manganese and nickel have also been reported in recent years.[46-48] While these examples demonstrate the great potential of MOFs as single site photocatalysts for CO_2 reduction, the selectivity and efficiency of most of these systems need to be improved.

Among the reported MOFs, UiO-series (UiO = University of Oslo) have high thermal and chemical stability, which are essential requirements of photocatalysts. The reports on modified UiO-68 for photoreduction are far fewer than UiO-66 and UiO-67.[49,50] However, the larger cavity and better CO_2 adsorbability imply that UiO-68 could be the ideal platform for photoreduction of CO_2. On the other hand, iron complexes have been shown to be efficient molecular catalysts for the CO_2-to-CO conversion.[51] Besides, the redox active 2,2′-bipyridine ligand can serve as electron reservoir and is expected to promote proton-coupled electron transfer (PCET) reactions through combining with iron.[52] Therefore, it is meaningful that Fe-bpy complex and UiO-68 MOF are selected to assemble an efficient photocatalyst for CO_2 reduction.

a. Coordination Chemistry Institute, State Key Laboratory of Coordination Chemistry, School of Chemistry and Chemical Engineering, Nanjing National Laboratory of Microstructures, Collaborative Innovation Center of Advanced Microstructures, Nanjing University, Nanjing 210023, China. E-mail address: sunwy@nju.edu.cn (W. Y. Sun);
b. Marquette University. Milwaukee, Wisconsin 53201, United States. E-mail: jier.huang@marquette.edu

Herein, we report a new MOF-based single site photocatalyst, i.e. UiO-68-Fe-bpy (bpy refers to 4′-methyl-[2,2′-bipyridine] moiety), synthesized based on UiO-68-NH$_2$ and 4′-methyl-[2,2′-bipyridine]-4-carbaldehyde (bpy-CHO) using an amine-aldehyde condensation and post-synthetic chelated metalation with FeCl$_3$ (Scheme 1). Under visible light illumination, we show that UiO-68-Fe-bpy can reduce CO$_2$ to form CO with excellent selectivity and demonstrate much better performance than its homogeneous counterpart with the same Fe(bpy)Cl$_3$ moiety. The enhanced photocatalytic performance of UiO-68-Fe-bpy can be attributed to the elongated excited state lifetime of Fe(bpy)Cl$_3$ moiety in UiO-68-Fe-bpy as confirmed by femtosecond transient absorption (TA) spectroscopy.

Experimental

Synthesis of UiO-68-Fe-bpy. The as-synthesized UiO-68-NH$_2$ (0.03 mmol, 0.08 g) was suspended in MeOH (5 mL) under ultrasound, then bpy-CHO (0.81 mmol, 0.16 g) dissolved in MeOH (5 mL) and acetic acid (HOAc) (25 μL) was added. The mixture was refluxed at 70 °C for 24 h. Afterwards, the precipitate was collected by centrifugation and washed with abundant MeOH (three times) and dried in air. The new MOF particles were dispersed into MeOH (10 mL), FeCl$_3$ (1.54 mmol, 0.25 g) was added, and the mixture was heated at 70 °C for additional 12 h. The resulting precipitate was collected by centrifugation and washed with abundant MeOH (three times) and dried in vacuum. IR (KBr pellet cm^{-1}) 3429 (m), 1700 (m), 1600 (vs), 1533 (m), 1420 (s), 1182 (w), 1104 (w), 785 (m), 713 (w), 657 (m), 567 (w), 467 (w).

Photochemical CO$_2$ reduction experiments. The photocatalytic activities of all samples were carried out in a batch-type reaction system (CEL-SPH2N-D9, CeAulight, China) equipped with a homemade photoreactor and a homemade circulating water filter to avoid photothermal effect. 2 mg sample was scattered in 1 mL acetone and ultra-sonicated for 5 minutes, then the suspension was uniformly dispersed onto a glass fiber film (Φ 25 mm, 0.22 μm pore diameter) drop by drop under infrared lamp. The film was activated in vacuum at 120 °C for 12 h. Then the film was fixed in the reaction cell, 2 mL of triethanolamine (TEOA) was added into the reactor, and the reactor was held at 50 °C by oil bath. After complete evacuation of the reaction system (no O$_2$ or N$_2$ could be detected), 80 kPa of pure CO$_2$ gas (99.999%, Tianhong Gas) was injected into the airtight system. A 300 W xenon arc lamp (Sirius-300P, Zolix Instruments Co., Ltd., China) with a 400-780 nm filter (CeAulight, China) was used as the light source. The optical power density was set at 200 mW cm^{-2} measured by optical power meter (CEL-NP2000-2, CeAulight, China). The gas products were monitored using gas chromatography (GC-9860, Luchuang Instrument, China), equipped with a TCD detector to measure H$_2$, and a FID detector with a methane conversion oven to convert CO and CO$_2$ into CH$_4$ before entering FID detector. The gas was separated by a 1 m TDX-01 column with N$_2$ (99.999%) as carrier gas, the temperature for TCD, FID, column and methane converter were 100, 150, 100 and 360 °C, respectively. The retention times of CO, CH$_4$ and H$_2$ are 1.290, 2.540 and 0.578 min, respectively. Calibration curves for gases were established separately.

Femtosecond optical ultrafast spectroscopy. Femtosecond OTA setup is based on a regenerative amplified Ti-Sapphire laser

system (Solstice, 800nm, < 100 fs FWHM, 3.5 mJ/pulse, 1 KHz repetition rate). The tunable (235−1100 nm) pump was generated by TOPAS from seventy-five percent of the Solstice output and was chopped at 500 Hz. The remaining twenty-five percent of the Solstice output was used to generate white light in a sapphire crystal (420−800 nm) in a Helios ultrafast spectrometer (Ultrafast Systems LLC). To make thin films for TA measurements, 1 mg of sample was added into 0.5 mL of Nafion (5% w/w in water and 1-propanol) in a glass vial. The hybrid was stirred for 2 h and then distributed uniformly on a piranha-etched glass. The samples were dried in air. The film samples were constantly translated in case of heating and permanent degradation. The pump power at 440 nm is 0.2 mW for all measurements.

Results and discussion

Synthesis of UiO-68-Fe-bpy

Briefly, the yellowish crystalline UiO-68-NH$_2$ was obtained by solvothermal reaction of amino-triphenyldicarboxylic acid (NH$_2$-TPDC) and ZrCl$_4$ in DMF in the presence of HOAc as a modulator.[53,54] UiO-68-NH$_2$ was then treated with bpy-CHO (excess) and HOAc in MeOH at 70 °C for 24 h to afford UiO-68-bpy via an amine-aldehyde condensation. UiO-68-Fe-bpy was achieved by metalation of UiO-68-bpy using FeCl$_3$ (Scheme 1).
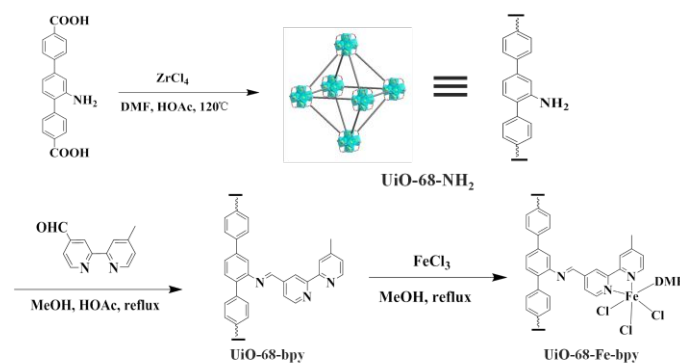
Scheme 1. Synthetic scheme of UiO-68-Fe-bpy.

The powder X-ray diffraction (PXRD) patterns of the as-synthesized UiO-68-NH$_2$ and post-modified UiO-68-Fe-bpy agree well with the simulated pattern of UiO-68-NH$_2$ (Fig. 1a), implying that the crystallinity of UiO-68-NH$_2$ retains during the PSM reaction. The SEM images show that UiO-68-NH$_2$ particles are discrete octahedral crystals with dimensions of 2 to 3 μm per side (Fig. 1b). The post-modified UiO-68-Fe-bpy shows similar morphology as its parent MOF (Fig. 1c), which further supports that UiO-68-NH$_2$ is chemically stable during the PSM. The inductively coupled plasma (ICP) measurement of Zr:Fe ratio of the digested UiO-68-Fe-bpy is 1:0.59 (Calcd 1:1), namely the functionalization yield is 59%, which is reasonable as reported previously.[54] We tried by varying the reactant ratio, reaction temperature and time to improve the functionalization yield, and finally got the highest yield of 59%. The limited modification yield may be ascribed to the heterogeneous PSM reaction.
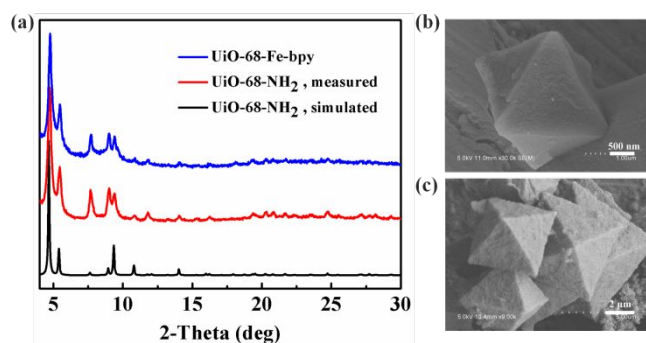
Fig. 1 (a) PXRD patterns of simulated and measured UiO-68-NH₂ and UiO-68-Fe-bpy. SEM images of (b) UiO-68-NH₂ and (c) UiO-68-Fe-bpy.

FT-IR spectra of UiO-68-NH₂ and UiO-68-Fe-bpy in the range of 4000-400 cm^{-1} shown in Fig. S1, ESI† demonstrate the formation of covalent modified compound. The FT-IR spectrum of UiO-68-NH₂ shows bands at 830 and 1580 cm^{-1} corresponding to the primary amino in- and out-of-plane bending vibrations, respectively.[55] After the amine-aldehyde condensation, the intensity of these characteristic amino peaks decreases. In contrast, the intensity of the peak at 1610 cm^{-1} associated with the N=C stretching vibration increases.[56] These changes imply that the UiO-68-NH₂ was successfully modified by amine-aldehyde condensation to generate UiO-68-bpy. In addition, ¹H NMR spectral measurements in DMSO-d_6 for digested UiO-68-NH₂ (Fig. S2a, ESI†) and UiO-68-bpy (Fig. S2b, ESI†) with aqueous HF were performed. The average integration ratio of signals originated from the bpy-CHO and NH₂-TPDC observed for the digested UiO-68-bpy sample (Fig. S2b, ESI†) is 0.62, implying that the functionalization yield by bpy-CHO is 62% agreeing with the ICP result of Fe-Zr ratio, which further confirms the successful combination of bpy-CHO with UiO-68-NH₂. Thermogravimetric analysis (TGA) was performed to examine the thermal stability of the frameworks. The TG curves of UiO-68-NH₂ and UiO-68-Fe-bpy show that they have similar thermal stability (Fig. S3, ESI†).

Fig. 2 (a) XANES and (b) Fourier-transformed EXAFS spectra of UiO-68-Fe-bpy and TPDC-Fe-bpy at Fe K-edge. The inset in (a) illustrates the first derivative of the XANES edges. The solid lines and open circles in (b) are experimental and fitted results, respectively.

In addition to the bulk structure, the local geometry of Fe center was examined by steady-state X-ray absorption spectrum (XAS). The control sample was TPDC-Fe-bpy synthesized by the

reaction of dimethyl ester of amino-triphenyldicarboxylic acid (amino-TPDC), bpy-CHO and FeCl₃ using the method for the preparation of UiO-68-Fe-bpy (Fig. S4, ESI†). Fig. 2a shows the XANES (X-ray absorption near edge structure) spectra of UiO-68-Fe-bpy and TPDC-Fe-bpy measured at Fe edge. The XANES spectrum of reference sample (FeCl₃ with octahedral geometry) was also shown in Fig. 2a. The main feature observed at 7121.13 eV is assigned to the dipole allowed 1s-4p transition. Additionally, the spectrum of FeCl₃ exhibits a sharp pre-edge feature corresponding to the quadrupole allowed 1s-3d transition and is forbidden for a perfect centrosymmetric octahedral geometry, which suggests the distorted octahedral geometry of Fe center in FeCl₃. The XANES spectrum for TPDC-Fe-bpy is similar to that of FeCl₃. However, there are some differences between the spectra of UiO-68-Fe-bpy and TPDC-Fe-bpy, including the intensity change of the so called B-feature (dashed line in Fig. 2a), and the different shape and intensity of absorption peak at region C compared to that of FeCl₃ and TPDC-Fe-bpy. These differences were established as a structure sensitive multiple scattering resonance previously,[57,58] implying that Fe center in UiO-68-Fe-bpy sample likely adopts a more distorted octahedral geometry. Moreover, the edge energy of both samples, as shown in the first derivative spectra (the inset of Fig. 2a), exhibits good agreement with FeCl₃ reference sample, suggesting that the Fe center retains +3 oxidation state after incorporation.

To gain more insight in the coordination environment, we quantitatively analyzed the extended X-ray absorption fine structure (EXAFS) spectra (Fig. S5, ESI†) with FeFF model. Fig. 2b shows the EXAFS spectra of UiO-68-Fe-bpy and TPDC-Fe-bpy in R-space. Compared to the spectrum of TPDC-Fe-bpy, the intensity of the peak corresponding to Fe-ligand first shell (eg. Fe-N and Fe-Cl) in the spectrum of UiO-68-Fe-bpy is reduced, which can be either attributed to the decreasing Fe coordination number or increasing disorder. It is unlikely that the coordination number of Fe changes. As a result, the decreased amplitude for Fe-ligand first shell peak can be attributed to the increased disorder of Fe coordination environment in UiO-68-Fe-bpy, consistent with XANES results. In addition, slight reduction of the bond distance of Fe-ligand first shell in UiO-68-Fe-bpy was observed compared to that of TPDC-Fe-bpy. These results are further supported by the fitting results. The best fitting to the EXAFS experimental data was also shown in Fig. 2b with the fitting parameters listed in Tables S1 and S2, ESI†, from which we found that the Fe-N distance of UiO-68-Fe-bpy (2.07 Å) is reduced by 0.04 Å compared to that of TPDC-Fe-bpy (2.11 Å). In contrast, while the Fe-Cl distance remains the same (2.18 Å) for both samples, the debye-waller factor increases slightly in UiO-68-Fe-bpy sample with respect to TPDC-Fe-bpy, consistent with the assignment of increasing disorder. These results together suggest that the coordination geometry for Fe center in UiO-68-Fe-bpy is largely similar to that of TPDC-Fe-bpy except for slightly reduced Fe-N distance and increased disorder for Fe-Cl.

X-ray photoelectron spectroscopy (XPS) was employed to explore the elemental composition of UiO-68-Fe-bpy (Fig. S6, ESI†). The peaks at 710.1, 531.6, 400.1, 284.5 and 184.5 eV correspond to the Fe 2p, O 1s, N 1s, C 1s and Zr 3d, respectively. Furthermore, peak-fitted N 1s core-line spectrum of UiO-68-Fe-bpy (Fig. S7, ESI†) shows the existence of three resolved peaks at 400.4, 399.6 and 398.9 eV, corresponding to the imine (-C=N-), amino (-
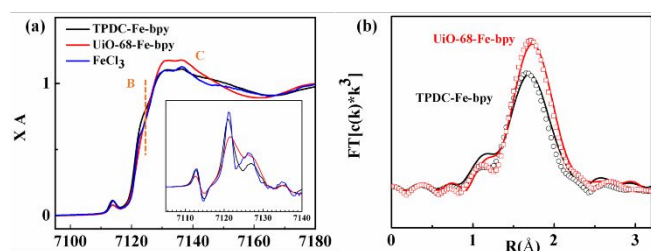
NH$_2$) and pyridine N, respectively.[55] Furthermore, the energy dispersive spectroscopy (EDS) spectra (Fig. S8, ESI†) of UiO-68-Fe-bpy disclosed the presence of metal element and the element mapping indicates that the Fe was modified uniformly throughout the MOF. The atomic ratio of Zr and Fe from EDS is estimated to be 1:0.51, which is close the result of ICP.

Gas adsorption properties of the guest-free UiO-68-NH$_2$ and UiO-68-Fe-bpy were examined to ensure the architectural stability and porosity after PSM. N$_2$ and CO$_2$ adsorption isotherms are shown in Figs. S9-S13, ESI†. As expected, the results indicate a decrease in porosity after PSM (Fig. S13, ESI†) with Brunauer-Emmett-Teller (BET) surface areas of 2589.7 and 1372.1 m^2/g for UiO-68-NH$_2$ (Fig. S9, ESI†) and UiO-68-Fe-bpy (Fig. S10, ESI†), respectively, which can be attributed to the introduction of Fe(bpy)Cl$_3$ moiety to the functional ligand of UiO-68-NH$_2$.[59]

With PSM of Fe(bpy)Cl$_3$ moiety into the UiO-68-NH$_2$, it is expected that UiO-68-Fe-bpy can improve the absorption capacity of visible light compared to the UiO-68-NH$_2$ since the absorption region of TPDC-Fe-bpy extends to 750 nm, which means that TPDC-Fe-bpy (ca. 1.69 eV) has great capacity to absorb visible light (Fig. S14, ESI†). Indeed, the color change from yellow to dark red after metalation was observed due to the coordination of Fe(III) with N atoms of bpy and the presence of ligand-to-metal (bpy→Fe^{III}) charge transfer (LMCT), from which corresponding electronic edge energy (Eg) of LMCT transitions can be estimated.[60] UV-Vis diffuse-reflectance spectra (DRS) show that the synthesized UiO-68-NH$_2$ (ca. 2.67 eV) and UiO-68-Fe-bpy (ca. 1.87 eV) have a similar absorption band in the region of 250-380 nm (Figs. S14 and S15, ESI†), which can be ascribed to the absorption of the Zr-O cluster.[61] However, UiO-68-Fe-bpy exhibits an extra absorption band with edge extending to around 700 nm in the visible light region, in agreement with the dark red color. These results suggest that UiO-68-Fe-bpy exhibits better absorption capacity of visible light after PSM.

Electrochemical properties of TPDC-Fe-bpy were investigated by cyclic voltammetry (Fig. S16, ESI†) in 0.1 M n-Bu$_4$NPF$_6$/DMF supporting electrolyte saturated with CO$_2$. When the electrochemical potential is scanned in the reductive direction, three distinct redox waves at -0.012 (process 1), -0.626 (process 2) and -0.971 (process 3) V versus SCE were observed, which can be attributed to Fe(III/II), Fe(II/I) and Fe(I/0).[62] As shown in Fig. S17, ESI†, compared to a N$_2$ atmosphere, the redox couple Fe(II/I) becomes irreversible, which suggests that Fe(I) can have interaction with CO$_2$ (Scheme S1). The excited state potential (E^*) of the UiO-68-Fe-bpy was estimated from the equation $E^* = E_{(Fe\ II/\ I)} + Eg$, where $E_{(Fe\ II/\ I)}$ is the ground state potential and Eg is the above-mentioned electronic edge energy. E^* was calculated to be about 1.24 V, implying that the electrons can be transferred from UiO-68-Fe-bpy to CO$_2$.[63] The results together suggest that UiO-68-Fe-bpy has the appropriate energetics and redox properties to catalyze the photocatalytic reduction of CO$_2$ to form CO.

Photochemical CO$_2$ conversion experiments

With successful modification of the Fe(bpy)Cl$_3$ into the robust MOF UiO-68-NH$_2$ and the feasibility as photocatalysts for CO$_2$ reduction, we evaluated the activity and selectivity of UiO-68-Fe-bpy for photocatalytic CO$_2$ reduction in the presence of TEOA as electron

donor upon visible light irradiation. As shown in Fig. S18, ESI†, FID detector, which monitors CO and CH$_4$, showed that CO was detected with retention time of about 1.290 min while no CH$_4$ (retention time: 2.540 min) was detected. On the other hand, TCD detector, which monitors H$_2$ generation, showed that no H$_2$ (retention time: 0.578 min) was detected. Besides, ^{1}H-NMR spectrum was used to detect the liquid product from the photocatalytic reaction and the results show no liquid product produced in the reaction system (Fig. S19, ESI†). These results together suggest that the selectivity of CO$_2$ photo-reduction to CO is 100%. Such high selectivity may be due to the solvent-free photocatalytic reaction system as reported previously,[64] in which TEOA acts as electron and proton donors and is oxidized to 2-(bis(2-hydroxyethyl)amino)acetaldehyde.[65] As shown in Fig. 3a, the control experiment with Xe lamp off shows that CO$_2$ to CO did not occur, suggesting that this reaction is light-driven. When the system was operated in the presence of UiO-68-NH$_2$ under visible-light illumination, CO$_2$ was split into CO at a reaction evolution of 10.01 μmol/g for six hours. Compared to the poor activity of UiO-68-NH$_2$, UiO-68-Fe-bpy exhibits much better photocatalytic efficiency (about 10 times of UiO-68-NH$_2$, Fig. 3a), suggesting that the incorporated Fe(bpy)Cl$_3$ plays a critical role in improving its photocatalytic activity. It is noteworthy that the photocatalytic efficiency of UiO-68-Fe-bpy is better than some typical MOFs and inorganic materials (Table S3, ESI†). Moreover, the photocatalytic performance of the physical mixture of TPDC-Fe-bpy and UiO-68-NH$_2$ was evaluated under the same catalytic conditions. As shown in Fig. 3a, the system stopped generating CO after three hours upon visible-light illumination, while UiO-68-Fe-bpy can steadily generate CO for at least 6 hours, suggesting that UiO-68-NH$_2$ can improve the stability of Fe(bpy)Cl$_3$, and the CO$_2$ reduction activity of UiO-68-Fe-bpy is not a simple sum of Fe-bpy and UiO-68-NH$_2$ activities. The covalent linkage of C=N between UiO-68-NH$_2$ and bpy could provide the ideal stability of UiO-68-Fe-bpy after PSM, which can prevent Fe complex from decomposing upon visible light illumination.[66] A proposed mechanism for photocatalytic CO$_2$ reduction over the UiO-68-Fe-bpy under visible light is provided in Scheme S1. Furthermore, the recycling experiments show that negligible change was observed in the CO-production yield during the three runs for 18 h (Fig. 3b). PXRD patterns (Fig. S20, ESI†) and SEM results (Fig. S21, ESI†) confirm that the crystallinity and structural integrity retain after photocatalytic reactions, suggesting that irradiation does not lead to catalyst photodegradation within 18 hours. The results of each cycle measured by ICP were shown in Table S4, ESI†.
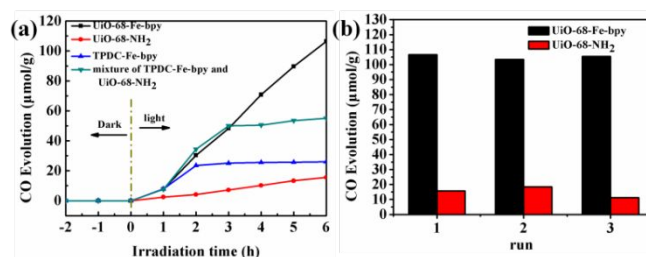

Fig. 3. (a) Photocatalytic CO evolution of UiO-68-NH$_2$, TPDC-Fe-bpy and UiO-68-Fe-bpy (2 mg photocatalyst). (b) Recycling performance of UiO-68-NH$_2$ and UiO-68-Fe-bpy.

Femtosecond optical ultrafast spectroscopy characterization

While the capability of UiO-68-Fe-bpy MOF as efficient photocatalysts for CO_2 reduction has been successfully demonstrated by the above photocatalytic experiments, it is necessary to study the excited state (ES) dynamics in order to figure out the specific roles that MOFs play in catalytic reaction. Femtosecond transient absorption (TA) spectroscopy was used to investigate the ES dynamics of UiO-68-Fe-bpy MOF. Fig. 4a and 4b shows the TA spectra of TPDC-Fe-bpy on Al_2O_3 film and UiO-68-Fe-bpy MOF following 400 nm excitation, respectively. Al_2O_3 film was used as a control to illustrate the intrinsic effect of porous surface on ES dynamics. As shown in Fig. 4a, the spectrum of TPDC-Fe-bpy exhibits a negative band centered at 570 nm, which can be assigned to the ground state bleach (GSB). At early time (< 2 ps), two positive features identified as ES absorption were observed at 460-500 nm and 650-800 nm regions. The ES signal at 460-500 nm was quickly replaced by the negative feature, which can be attributed to the

overlap of ES absorption with GSB and the faster decay of ES than the GSB recovery. Compared to TPDC-Fe-bpy, UiO-68-Fe-bpy shows similar GSB centered at 600 nm, which is consistent with UV-Vis ground state absorption spectrum. However, distinct differences were observed between the GSB recovery kinetics of two samples. As shown in Fig. 4c, the recovery of GSB in UiO-68-Fe-bpy is slower compared to TPDC-Fe-bpy on Al_2O_3 film, which suggests that the recovery of ES molecules to the ground state was inhibited in UiO-68-Fe-bpy and thus a longer lived ES of Fe complex in UiO-68-Fe-bpy. One possible explanation for the elongated ES lifetime is that the rigid framework plays an important role in stabilizing the charged separated excited state and suppressing the undesired charge recombination, which has also been observed in previously published work.[67] Therefore, the long ES lifetime of a photocatalyst is beneficial for charge transfer from the sacrificial donor to the catalyst or from the catalyst to reduce CO_2, which well explains the enhanced catalytic performance of UiO-68-Fe-bpy with respect to TPDC-Fe-bpy for CO_2 reduction.
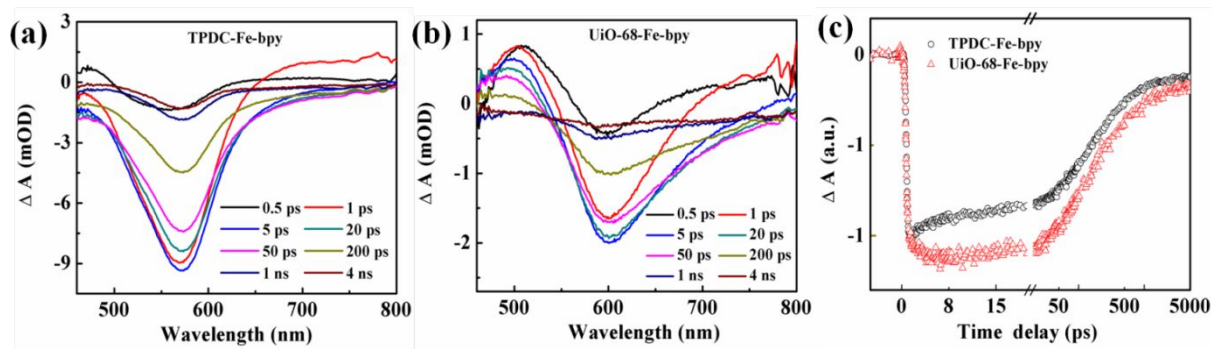

Fig. 4. Femtosecond TA spectra of (a) TPDC-Fe-bpy and (b) UiO-68-Fe-bpy. (c) Comparisons of the ground state bleach (GSB) recovery between TPDC-Fe-bpy and UiO-68-Fe-bpy.

Conclusions

In summary, we have successfully synthesized a MOF photocatalyst by incorporating $Fe(bpy)Cl_3$ using PSM, which shows enhanced light-absorbing ability and serves as highly efficient CO_2 reduction to form CO with 100% selectivity under visible-light irradiation. Using transient absorption spectroscopy, we show that $Fe(bpy)Cl_3$ in UiO-68-NH_2 has longer-lived ES and slower recovery of GSB, which is beneficial for boosting the efficiency of photocatalytic CO production. In addition, the robust nature of UiO-68 ensured the stability of the photocatalyst (UiO-68-Fe-bpy), enabling at least three cycles (18 h) of photocatalytic process. This work not only reports a new MOF photocatalyst for CO_2 reduction with perfect selectivity for CO generation but also elucidates that PSM is an effective strategy to introduce molecular metal complex to optimize MOF-based materials for photocatalysis.

Acknowledgements

Notes and references

1   J. Artz, T. E. Muller, K. Thenert, J. kleinekorte, R. Meys, W. Leitner. *Chem. Rev.* 2018, **118**, 434–504.
2   J. Di, C. Zhu, M. Ji, M. Duan, R. Long, C. Yan, K. Gu, J. Xiong, Y. She, J. Xia, H. Li, Z. Liu, *Angew. Chem. Int. Ed*. 2018, **57**, 14847-14851.
3   C. Hu, X. Hu, R. Li, Y. Xing, *J. Hazard. Mater*. 2020, **385**, 121599-121603.
4   T. Kajiwara, M. Fujii, M. Tsujimoto, K. Kobayashi, M. Higuchi, K. Tanaka, S. Kitagawa, *Angew. Chem. Int. Ed*. 2016, **55**, 2697-2700.
5   R. Heng, S. Lucianac, B. Julien, R. Marc, *Nature* 2017, **548**, 74-77.
6   Y. Huang, Z. Guo, H. Liu, S. Zhang, P. Wang, J. Lu, Y. Tong, *Adv.*

Funct. Mater. 2019, **29**, 1903490-1903499.

7   M. Matsuoka, M. Anpo, *Photochem. Photobiol. C* 2003, 3, 225-252.

8   W. Lin, H. Frei, *J. Am. Chem. Soc.* 2005, **127**, 1610-1611.

9   S. Habisreutinger, L. Schmidt-Mende, J. Stolarczyk, *Angew. Chem. Int. Ed.* 2013, **52**, 7372-7408.

10 Y. Tamaki, T. Morimoto, K. Koike, O. Ishitani, *Proc. Natl. Acad. Sci. U.S.A.* 2012, **109**, 15673-15678.

11 S. Sato, T. Morikawa, T. Kajino, O. Ishitani, *Angew. Chem. Int. Ed.* 2013, **52**, 988-992.

12 V. Sara, N. Kornienko, C. Margarit, P. Yang, C. Chang, *J. Am. Chem. Soc.* 2013, **135**, 14413-14424.

13 A. Morris, G. Meyer, E. Fujita, *Acc. Chem. Res.* 2009, **42**, 1983-1994.

14 Y. Qu, X. Duan, *Chem. Soc. Rev.* 2013, **42**, 2568-2580.

15 A. McKinlay, R. Morris, P. Horcajada, G. Ferey, R. Gref, P. Couvreur, C. Serre, *Angew. Chem. Int. Ed.* 2010, **49**, 6260-6266.

16 K. Taylor-Pashow, J. DellaRocca, Z. Xie, S. Tran, W. Lin, *J. Am. Chem. Soc.* 2009, **131**, 14261-14263.

17 L. Murray, M. Dinca, J. Long, *Chem. Soc. Rev.* 2009, **38**, 1294-1314.

18 J. Rowsell, O. Yaghi, *Angew. Chem. Int. Ed.* 2005, **44**, 4670-4679.

19 R. Matsuda, R. Kitaura, S. Kitagawa, Y. Kubota, R. Belosludov, T. Kobayashi, H. Sakamoto, T. Chiba, M. Takata, Y. Kawazoe, Y. Mita, *Nature* 2005, **436**, 238-241.

20 J. Lang, Q. Xu, R. B. Yuan, Abrahams, *Angew. Chem. Int. Ed.* 2004, **43**, 4741-4745.

21 D. Liu, J. Lang, B. Abrahams, *J. Am. Chem. Soc.* 2011, **133**, 11042–11045.

22 L. Bastin, P. Brcia, E. Hurtado, J. Silva, A. Rodrigues, B. Chen, *J. Phys. Chem. C* 2008, **112**, 1575-1581.

23 Y. Shi, W. Zhang, B. Abrahams, P. Braunstein, J. Lang, *Angew. Chem. Int. Ed.* 2019, **58**, 9453–9458.

24 F. Li, Q. Shao, X. Huang, J. Lang, *Angew. Chem. Int. Ed.* 2018, **57**, 1888-1892.

25 F. Li, P. Wang, X. Huang, D. Young, H. Wang, P. Braunstein, J. Lang, *Angew. Chem., Int. Ed.* 2019, **58**, 7051-7056.

26 F. Hu, Y. Mi, C. Zhu, B. Abrahams, P. Braunstein, J. Lang, *Angew. Chem. Int. Ed.* 2018, **57**, 12696-12701.

27 A. Corma, H. Garcia, F. Xamena, *Chem. Rev.* 2010, **110**, 4606-4655.

28 J. Lee, O. Farha, J. Roberts, K. Scheidt, S. Nguyen; J. Hupp, *Chem. Soc. Rev.* 2009, **38**, 1450-1459.

29 Y. Fu, D. Sun, Y. Chen, R. Huang, Z. Ding, X. Fu, Z. Li, *Angew. Chem. Int. Ed.* 2012, **51**, 3364 –3367.

30 Y. Chen, D. Wang, X. Deng. Z. Li, *Catal. Sci. Technol.* 2017, **7**, 4893-4904.

31 D. Wang, R. Huang, W. Liu, D. Sun, Z. Li, *ACS Catal.* 2014, **4**, 4254-4260.

32 C. Wang, Z. Xie, K. EdeKrafft, W. Lin, *J. Am. Chem. Soc.* 2011, **133**, 13445-13454.

33 T. Toyao, M. Saito, S. Dohshi, K. Mochizuki, M. Iwata, H. Higashimura, Y. Horiuchi, M. Matsuoka, *Chem. Commun.* 2014, **50**, 6779-6781.

34 Y. Lin, C. Kong, Q. Zhang, L. Chen, *Adv. Energy Mater.* 2017, **7**, 1601296.

35 E. Sanz-Perez, C. Murdock, S. Didas, C. Jones, *Chem. Rev.* 2016, **116**, 11840-11876.

36 J. Liu, P. Thallapally, B. McGrail, D. Brown, *Chem. Soc. Rev.* 2012, **41**, 2308-2322.

37 Y. Bae, R. Snurr, *Angew. Chem. Int. Ed.* 2011, **50**, 11586-11596.

38 X. Deng, Y. Qin, M. Hao, Z. Li, *Inorg. Chem.* 2019, **58**, 16574-16580.

39 D. Sun, Y. Gao, J. Fu, X. Zeng, Z. Chen, Z. Li, *Chem. Commun.* 2015, **51**, 2645-2648.

40 X. Deng, J. Albero, L. Xu, H. García, Z. Li, *Inorg. Chem.* 2018, **57**, 8276-8286.

41 C. Cohen, T. Chu, G. Coates, *J. Am. Chem. Soc.* 2005, **127**, 10869-10878.

42 J. Louie, J. Gibby, M. Farnworth, T. Tekavec, *J. Am. Chem. Soc.* 2002, **124**, 15188-15189.

43 S. Xie, Q. Zhang, G. Liu, Y. Wang, *Chem. Commun.* 2016, **52**, 35-59.

44 S. K. Lee, M. Kondo, M. Okamura, T. Enomoto, G. Nakamura, S. Masaoka, *J Am Chem Soc*, 2018, **140**, 16899-16903.

45 R. Reithmeier, S. Meister, A. Siebel, B. Rieger, *Dalton Trans*. 2015, **44**, 6466-6472.

46 C. Cometto, R. Kuriki, L. Chen, K. Maeda, T. Lau, O. Ishitani, M. Robert, *J Am Chem Soc*, 2018, **140**, 7437-7440.

47 H. Takeda, H. Koizumi, K. Okamoto, O. Ishitani, *Chem Commun*, 2014, **50**, 1491-1493.

48 V. Sara, N. Kornienko, C. Margarit, P. Yang, C. Chang, *J Am Chem Soc*, 2013, **135**, 14413-14424.

49 X. Gao, B. Guo, C. Guo, Q. Meng, J. Liang, J. Liu, *ACS Appl. Mater. Interfaces* 2020, **12**, 24059-24065.

50 W. Liao, J. Zhang, Z. Wang, S. Yin, M. Pan, H. Wang, C. Su, *J. Mater Chem. A* 2018, **6**, 11337-11345.

51 H. Rao, L. Schmidt, J. Bonin, M. Robert, *Nature* 2017, **548**, 74–77.

52 P. Alsabeh, A. Hernández, E. Barsch, H. Junge, R. Ludwig, M. Beller, *Catal. Sci. Technol.* 2016, **6**, 3623-3630.

53 A. Schaate, P. Roy, A. Godt, J. Lippke, F. Waltz, M. Wiebcke, P. Behrens, *Chem. Eur. J.* 2011, **17**, 6643-6651.

54 Y. P. Wei, Y. Liu, F. Guo, X. Y. Dao; W. Y. Sun, *Dalton Trans*. 2019, **48**, 8221-8226.

55 J. Wang, M. Yang, W. Dong, Z. Jin, J. Tang, S. Fan, Y. Lu, G. Wang, *Catal. Sci. Technol.* 2016, **6**, 161-168.

56 L. Garzon, R. Hermida, I. Imaz, D. Maspoch, *J. Am. Chem. Soc.* 2017, **139**, 897-903.

57 C. Bressler, C. Milne, V. Pham, A. ElNahhas, C. Borca, C. Ingold, R. Abela, M. Chergui, *Science* 2009, **323**, 489-492.

58 V. Briois, P. Sainctavit, G. Long, F. Grandjean, *Inorg. Chem.* 2001, **40**, 912-918.

59 H. Fei, M. Sampson, L. Yeob, P. Kubiak, M. Cohen, *Inorg. Chem.* 2015, **54**, 6821-6828.

60 E. Ross-Medgaarden, I. Wachs, *J. Phys. Chem. C* 2007, **111**, 15089-15099.

61 D. Sun, Y. Fu, W. Liu, L. Ye, D. Wang, Z. Li, *Chem. Eur. J.* 2013, **19**, 14279-14285.

62 C. Cardona, W. Li, A. Kaifer, D. Stockdale, G. Bazan, *Adv. Mater.* 2011, **23**, 2367-2371.

63 R. Rodrigues, C. Boudreaux, E. Papish, J. Delcamp, *ACS Appl. Energy Mater.* 2019, **2**, 37-46.

64 X. Y. Dao, J. H. Guo, Y. P. Wei, F. Guo, Y. Liu, W. Y. Sun, *Inorg. Chem.* 2019, **58**, 8517-8524.

65 S. Q. Wang, X. Y. Zhang, X. Y. Dao, X. M. Cheng, W. Y. Sun, *ACS Appl. Nano Mater*. 2020, **3**, 10437-10445.

66 W. Wang, T. B. Rauchfuss, *J. Am. Chem. Soc.* 2012, **134**, 4525-4528.

67 L. Hanna, P. Kucheryavy, C. Liu, X. Zhang, J. Lockard, *J. Phys. Chem. C* 2017, **121**, 13570-13576.

Journal Name

ARTICLE

For Table of Contents Use Only:

Iron(III)-bipyridine incorporated metal-organic frameworks for photocatalytic reduction of CO$_2$ with improved performance

Yuan-Ping Wei, Sizhuo Yang, Peng Wang, Jin-Han Guo, Jier Huang* and Wei-Yin Sun*
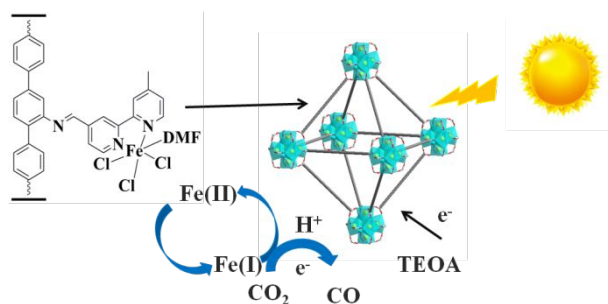
A novel MOF UiO-68-Fe-bpy was constructed through post-synthetic modification of Zr(IV)-based MOF UiO-68-NH$_2$ as a photocatalyst for CO$_2$ reduction.